metals

MDPI

Article

Effects of Warm Laser Peening on Thermal Stability and High Temperature Mechanical Properties of A356 Alloy

Hansong Chen [1], Jianzhong Zhou [1,*], Jie Sheng [1], Xiankai Meng [1], Shu Huang [1] and Xiaojiang Xie [2]

[1] School of Mechanical Engineering, Jiangsu University, Zhenjiang 212013, China; chenhs0701@sina.com (H.C.); shengjie686@sina.com (J.S.); mengdetiankong10@126.com (X.M.); huangshu11@sina.com (S.H.)

[2] College of mechanical and Electronic Engineering, Ji'an College, Ji'an 343000, China; xiexjiang@163.com

* Correspondence: zhoujz@ujs.edu.cn; Tel.: +86-511-8879-7063; Fax: +86-511-8878-0219

Academic Editor: Patrice Peyre

Received: 29 February 2016; Accepted: 25 April 2016; Published: 24 May 2016

Abstract: To study the effects of warm laser peening (WLP) on the thermal stability and mechanical properties of A356 alloy, the samples were treated by WLP using a Nd:YAG solid-state laser and temperature control device. The residual stress, micro-hardness and microstructures of samples treated by WLP were observed. The result shows that the temperature significantly affects the strengthening effect of laser peening (LP). The residual stress induced by WLP decreases with the increasing temperature. The micro-hardness and dislocation density increase first, and then decrease with the increases of temperature. The grain refinement degree of the samples treated by WLP is much higher than that of LP. In addition, after aging for 100 min at 220 °C, the samples treated by LP and WLP were comparatively investigated in thermal stability. Obviously, the residual compressive stress, micro-hardness and microstructure induced by WLP present a better thermal stability property than that of LP. The residual stress and micro-hardness of WLP samples are obviously improved, and the increasing degrees are 23.31% and 19.70%, respectively. The dislocation density remains at a high level, while the grains are still in fine crystalline state.

Keywords: warm laser peening; A356 alloy; residual stress; micro-hardness; mechanical property

1. Introduction

As a typical Al-Si alloy, A356 alloy plays an important role in the field of industry because of its excellent casting properties, low density, high wear resistance and low thermal expansion [1,2]. A356 alloys have been widely used in cylinder heads, engine blocks and cylinder liners [3–5]. However, the surface properties of A356 alloy are poor [6,7]. It has been proved that the main failure modes of A356 alloy during the service process are fatigue and wear failure, which are normally initiated on the surface. Therefore, researchers tried to use different surface treatment technologies, such as mechanical peening, micro-arc oxidation, surface alloying and friction stir welding, to improve the mechanical properties of A356 alloy [8–12]. Cho [13] used high energy peening to treat A356 alloy, and the results showed that after the treatment, the surface micro-hardness of A356 alloy was raised by 400% as compared to the initial matrix. In addition, the Si particles on the surface were significantly refined and balled. Chang [14,15] investigated the mechanical properties and thermal stability of A356 alloy treated by surface alloying technology. The results showed that a nano-grain structure was discovered in the treated area after 60 min, the size of which was about 18 nm. The surface micro-hardness was raised by 80% as compared to the initial matrix. Furthermore, the nano-grain structure presented good thermal stability after being maintained

at an elevated temperature. Mazaheri [16] used friction stir welding (FSW) technology to deposit the nano-Al_2O_3 particles on the A356 alloy surface layer. The results showed that the friction stir technology could remarkably improve the mechanical properties of A356 alloy, and the nano-grain structure was induced while a surface micro-hardness of 111 HV was achieved, raised 30% compared with the substrate. Lee [17] employed a micro-arc oxidation process to fabricate pure aluminum film on the A356/Al_2O_3 surface, and it showed that a film with a thickness of 100 μm was formed on the treated surface, and the wear rate and friction coefficient were significantly decreased, about 20 mg/km (1000 mg/km before treatment)and 0.3 (0.5 before treatment), respectively, at 180 °C. However, the complex process, high-tech requirements and poor flexible manufacturing limit the application of the above-mentioned methods.

Warm laser peening (WLP) is an advanced surface-strengthening treatment technique which was developed based on laser peening (LP). As an innovative thermo-mechanical treatment technique, it integrates the advantages of laser peening and dynamic strain aging (DSA) [18,19]. WLP increases the dislocation density of treated metals, pinning the mobile dislocations by solute atoms, and thus stabilizes the dislocation structure. During the WLP process, solute atoms migrate to dislocation cores, which form so-called Cottrell clouds [20]. The Cottrell clouds inhibit the dislocation movement during plastic deformation. In addition, WLP generates nano-scale precipitates through strain-induced precipitation [21–23], and the nano-scale precipitates distributed near the grain boundaries prevent the grain boundary from sliding. Ye's group had studied the fatigue life improvement of AA6061 induced by the WLP process at ambient temperature [19]. An initial conclusion was achieved that the thermal stability of the residual stress generated by WLP is much higher than that generated by LP. However, more data are required to support this viewpoint.

This paper aims to investigate the evolution of the residual stress, micro-hardness and microstructures of the A356 alloy before and after WLP. In particular, the thermal stability of some typical surface properties of the WLP-treated sample was revealed.

2. Experiments

2.1. Materials

A356 alloy was selected, the chemical composition and mechanical properties at room temperature of the A356 alloy are shown in Tables 1 and 2 respectively. The dimension and schematic diagrams of specimen are shown in Figure 1. Before WLP, all the specimens were polished by Al_2O_3 sandpaper with different grades of roughness (from 240# to 2000#), and then cleaned by acetone and industrial alcohol. Finally, all the samples were polished again by the automatic polishing machine.

Table 1. Chemical composition of A356 alloy (wt. %).

Elements	Si	Cu	Fe	Mn	Mg	Zn	Ti	Al
(wt. %)	6.5~7.5	0.2	0.2	0.1	0.25~0.45	0.1	0.08~0.2	balance

Table 2. Mechanical properties of A356 alloy at room temperature.

Mechanical Properties	Value
Tensile strength (MPa)	197
Yield strength (MPa)	168
Elongation (d, %)	6.1
Brinell hardness (HV)	80

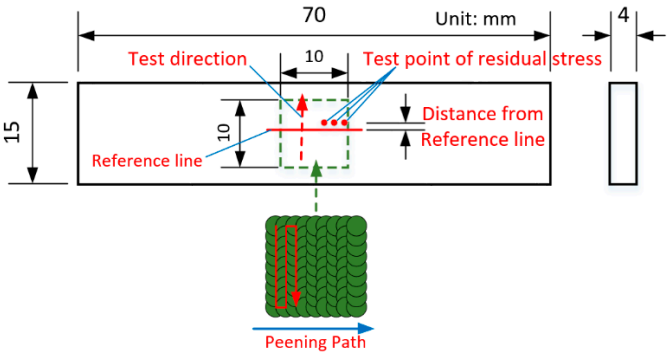

Figure 1. Shape and size diagram of rectangular samples and test solutions of residual stress.

2.2. Warm Laser Peening Experiments

A schematic of the WLP process is shown in Figure 2. BK7 glass was used as the confining medium because of its high shock impedance and high melting point. A thin black tape (thickness is 30 μm) was used as an ablative coating material to prevent the sample surface from melting. The working temperatures for WLP are controlled by a heating device which was developed by our group. A thermodetector was used to monitor the sample temperature. During WLP, the shock waves were induced by a Q-switched Nd-YAG laser with a wavelength of 1064 nm, pulse duration of 8 ns and a spot diameter of 2 mm. The laser energy is changed by adjusting the Q-switched delay time, the laser energy adopted was 1.8 J, working temperature was 25, 90, 120, 150, 180 and 210 °C, respectively, while the overlap ratio was 50%.

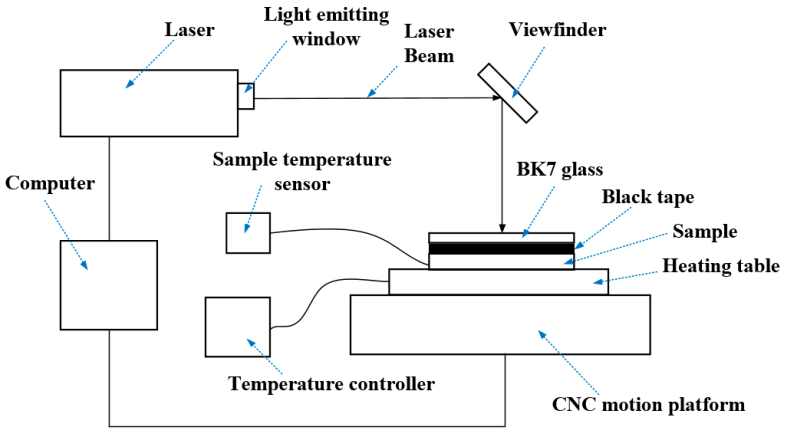

Figure 2. Schematic of the WLP process.

First, the rectangular samples were treated by WLP. The peening area was 10 × 10 mm, as seen in Figure 1. Then the micro-hardness and residual stress induced by WLP were tested. An optimum parameter of WLP was selected based on the previous test results. Furthermore, the microstructure of samples treated by WLP with the optimum parameter was observed. At last, a continuous high temperature aging experiment of samples treated by WLP with the optimum processing parameter and control group was conducted in the DGH-9030A electro-thermal bleat drying box (Yiheng Scientific Instrument Co., Ltd., Shanghai, China). The temperature used was 220 °C at a heating rate of 0.1 °C/s, cooled to room temperature inside the drying box.

2.3. Characterization

The residual stresses on the surface were measured by X-350A stress analyzer (Stress Technologies Co., Ltd., Handan, China). We use Cr Kα radiation and sin2ψ method to calculate the result.

The diameter of X-ray collimator (Stress Technologies Co., Ltd.) used in this work is 1 mm. The {311} peak was used for stress analysis, which corresponds to a 2θ angle of 138.862° in the unstressed state. The scanning start angle and end angle are 143° and 135°, respectively, ψ is 0°, 24°, 35° and 45°. The X-ray tube voltage is 22 kV, the current of which is 6.0 mA. The stress constant is −162 MPa/degree. Three points were selected, and the mean value of the three points was obtained as the final residual stress value. The testing schematic was shown in Figure 1. Because the residual stress in depth cannot be tested by X-ray diffraction (XRD), a XF-1 electrolytic polishing machine (Stress Technologies Co., Ltd.) was used to measure the residual stress in depth base on the electrolytic polishing method. The electrolyte matching was 10 mL perchloric acid and 90 mL alcohol. The polishing voltage was 20 V and the current was 0.8 A.

The micro-hardness of samples treated by WLP was measured by a Vickers micro-hardness tester (HXD-1000TM, Taiming Optical Instrument Co., Ltd., Shanghai, China) with a 200 gf load and a 10 s holding time. Each reported measurement is an average of three separate readings, as shown in Figure 3. The micro-hardness along the depth direction were tested, the selected depth are 50, 150, 300, 450, 600, 750 and 900 μm.

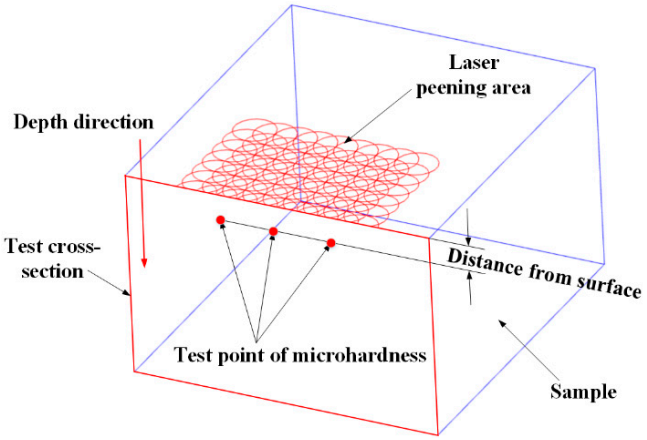

Figure 3. Test solutions of micro-hardness.

Using hydrofluoric acid with concentration of 10% to etch the samples treated by WLP with optimum parameters, the etching time was 40 s. The size and morphology of grains and distribution of surface Si particles were observed by LEICA DFC420 optical microscope (Leica Microsystems GmbH, Wetzlar, Germeny) and JSM-7001F Scanning Electron Microscope (SEM, JEOL Ltd., Tokyo, Japan) (accelerating voltage: 0.5–30 kV).

3. Results and Discussion

3.1. Residual Stress

The surface residual stress distribution of A356 alloy induced by WLP with different substrate temperature was shown in Figure 4. It can be seen that the residual compressive stress induced by laser peening at room temperature (25 °C) was average about −212.71 MPa. However, the compressive residual stresses decrease gradually with the increase of temperature. This result is coincident with the residual stress changing tendency of Ye's study about copper alloy treated by WLP [22].

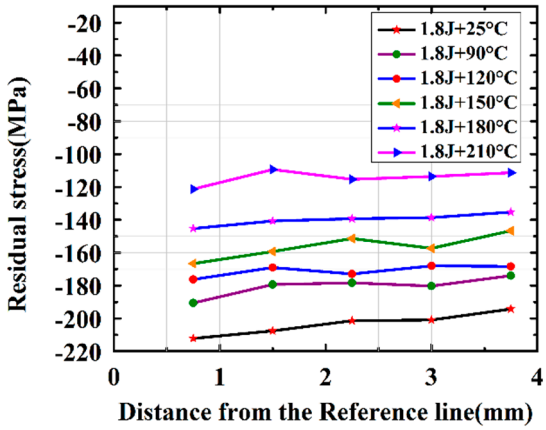

Figure 4. Surface residual stress distribution of WLP-treated samples at different temperatures.

As we know, the WLP-treated sample suffered an external temperature, inducing a softening effect [24]. As shown in Figure 4, due to the softening effect, WLP-induced dislocation accumulation may decrease with temperature, which results in a decrease of residual stress [21]. In addition, under high temperature, the kinetic energy of atoms inside the material, atomic motion and vibration amplitude will increase, and thus accelerate the high energy atomic lattice in reverting back to the equilibrium position quickly. Eventually, the lattice arrangement gradually balances, resulting in a decrease of the residual compressive stress.

3.2. Micro-Hardness

The micro-hardness of A356 alloy in the depth direction is shown in Figure 5.

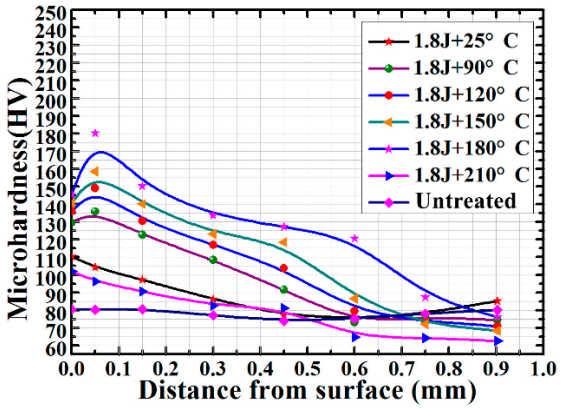

Figure 5. Hardness distribution in depth.

From Figure 5, we can observe that the micro-hardness and hardening layer depth are significantly changed before and after WLP. The average micro-hardness of the matrix without any treatment is about 80.01 HV. When the hardness is less than or equal to this average value, we consider it as the depth of the hardening. As seen in Figure 5, the micro-hardness increases initially, the maximum micro-hardness appears at a depth of 50 μm, then it decreases with the increasing temperature, and the depth of the hardening layer also increases with the increasing temperature. This phenomenon was not observed in LP temperature (25 °C) and above the DSA temperature (210 °C). For these two temperatures, the micro-hardness decreases from the beginning. The reason is that the hardening mechanism of the WLP process, which is different from that of LP, includes mechanical hardening, the DSA effect and thermal-assisted dynamic precipitation (DP) [21].

The maximum micro-hardness induced by WLP increases from 110.44 to 180.14 HV when the temperature changes from 25 to 180 °C, and the corresponding hardening layer depth increases from 0.42 to 0.86 mm. However, the micro-hardness rapidly decreases to a value of 101.98 HV when the temperature rises to 210 °C.

It is well known that the DSA phenomenon appears during the WLP process. The dislocation density of WLP-treated samples rapidly increases [25], while a large number sub-grain boundaries are formed, eventually refining the grain size. According to the Hall-Petch equation [26]:

$$Hv = Hv_0 + K_{Hv}d^{-1/2} \quad (1)$$

where Hv and Hv_0 are the micro-hardness of the treated sample and matrix, respectively, K_{Hv} is the Hall-Petch constant (for aluminum alloy, $K_{Hv} > 0$) [26], and d is the grain size. From the equation, Hv increases with the decrease of the grain size. This indicates that WLP induces a grain refinement effect, which may increase the hardness of treated samples, as seen in Figure 5. However, an extremely high temperature will cause uncontrolled grain growth, finally reducing the hardness.

3.3. Microstructure Analysis

According to the experimental results of residual stress and micro-hardness, a typical case with a laser energy of 1.8 J and a working temperature of 120 °C was picked in this study. The surface microstructure of WLP-treated samples at optimum parameters are shown in Figure 6. From Figure 6a, it can be seen that the grain size of the matrix was large, about 120 μm. After the LP treatment, the grain size is significantly refined, at about 65 μm, as shown in Figure 6b. However, when treated by WLP, the grain size in the peening area is further refined, as seen in Figure 6c. The grain size of WLP-treated samples decreases to 35 μm. This is mainly due to the dislocation caused by the dynamic strain aging pinning effect of the dislocation caused by the proliferation; the dislocation density increases, which leads to grain refinement.

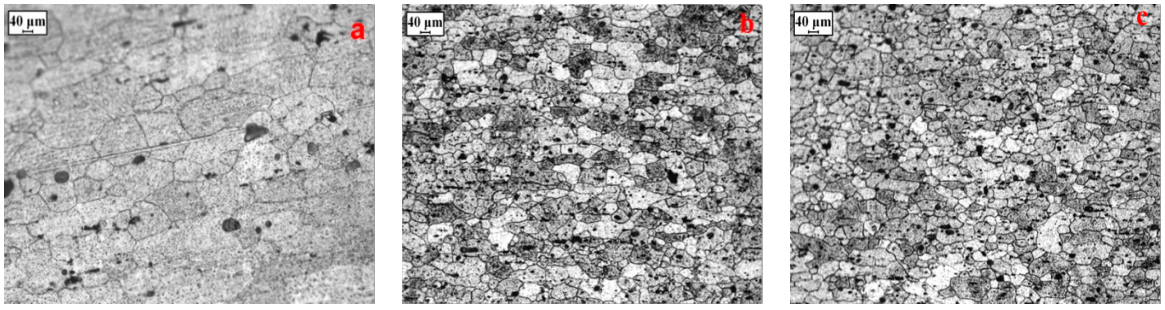

Figure 6. Microstructures of samples: (**a**) matrix; (**b**) LP-treated (1.8 J + 25 °C); (**c**) WLP-treated (1.8 J + 120 °C).

SEM morphologies of surface Si particles are shown in Figure 7. From Figure 7a, it is noted that the Si particles with coarse grains and strip shapes are randomly distributed on the surface. A shrinkage hole induced by casting remains on the surface. However, the size, the shape and the distribution of Si particles are obviously changed after the LP process, as seen in Figure 7b. The Si particles are significantly refined and balled, the initial long rod-like shape changes into the short shape, and the size of the shrinkage hole reduces as well. Furthermore, as seen in Figure 7c, compared with LP process, the Si particles are more deeply refined and balled, and the size of the shrinkage hole further reduces after WLP treatment, this may significantly improve the mechanical properties of the A356 alloy.

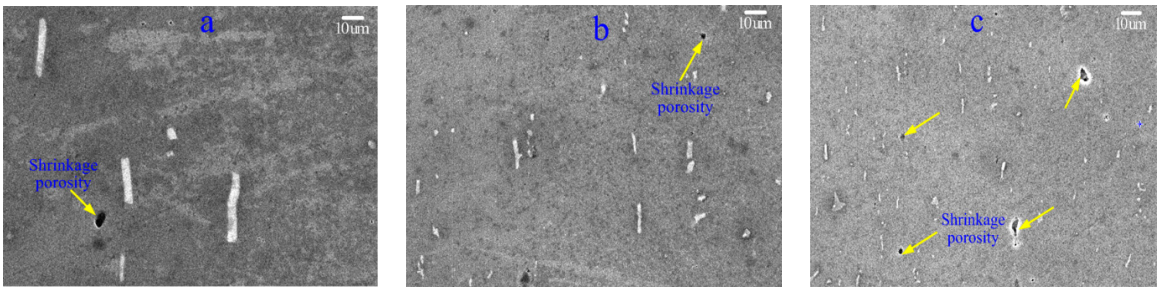

Figure 7. SEM morphologies of samples: (**a**) matrix; (**b**) LP-treated (1.8 J + 25 °C); (**c**) WLP-treated (1.8 J + 120 °C).

3.4. Thermal Stability Test

To easily record results, warm laser peening-treated samples (1.8 J/120 °C), laser peening-treated samples (1.8 J/25 °C) and matrix are identified as WLP, LP and MA, respectively.

3.4.1. Residual Stress

The surface residual stress distribution curves of WLP, LP and MA samples after aging for 100 min at 220 °C are shown in Figure 8.

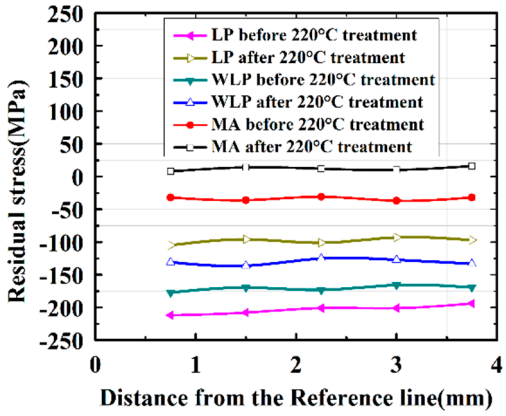

Figure 8. Surface residual stress distribution of samples after high temperature aging.

From the chart, it can be seen that the maximum residual stress of the matrix changes from residual compressive stress (−32.11 MPa) to tensile stress (12.23 MPa). The maximum residual stress of WLP-treated samples reduces from −177.62 to −136.21 MPa, achieving a reduction of 23.31%, while this value of LP-treated samples reduces from −212.71 to −104.91 MPa, achieving a reduction of 50.68%. This indicates that the thermal stability of residual stress induced by WLP is higher than that of LP. The better thermal stability may contribute to the good thermal stability of dislocation induced by WLP.

The residual stress distribution curves in depths of the WLP, LP and MA samples after aging 100 min at 220 °C are shown in Figure 9. From the chart, we can see that the effect layer depths of the residual compressive stress induced by WLP and LP reach 0.65 and 0.42 mm, respectively, before thermal insulation. However, after aging, the effect layer depth of the residual compressive stress induced by WLP is still maintained at 0.52 mm, while this value decreases to 0.28 mm for LP-treated samples. That means the decreasing rate of WLP and LP after aging is 20% and 33%, respectively. These results show that the residual stress induced by WLP is deeper and more stable than LP, and this trend still exists after aging, although the changes in the absolute value of the effect layer depth are nearly the same.

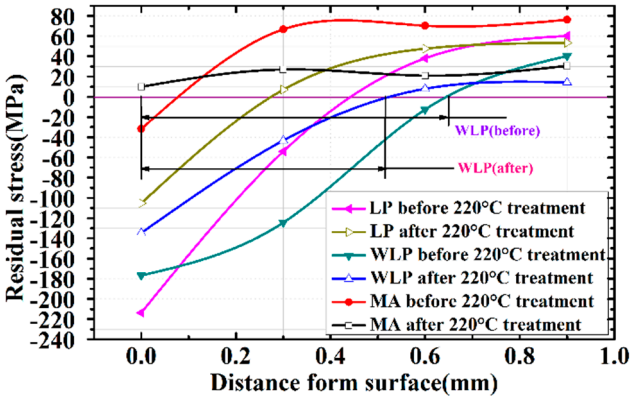

Figure 9. Residual stress distribution in depth of samples before and after aging.

3.4.2. Micro-Hardness

The surface micro-hardness distribution curves of the WLP, LP and MA samples after aging for 100 min at 220 °C are shown in Figure 10. It can be seen that the micro-hardness induced by WLP has good thermal stability. After aging, the micro-hardness of the matrix reduces from 80.01 to 46.34 HV (33.67 HV decreased), achieving a reduction of 42.08%, while this value for LP-treated samples decreases from 110.44 to 71.57 HV (38.87 HV decreased), achieving a reduction of 35.20%. However, for WLP-treated samples, the reduction in micro-hardness is minor. The value reduces from 149.01 to 119.66 HV (29.35 HV decreased), decreasing by 19.70%. Similar to the variation of residual stress in depth, the changes in the absolute value of micro-hardness are about the same after aging, but the micro-hardness induced by WLP is higher and more stable than that induced by LP.

The advantage of the WLP process can be reflected by the good thermal stability of the residual stress and micro-hardness induced by WLP. We can infer that the dislocation induced by WLP has an excellent thermal stability, and the precipitates formed by DP are segregated near the grain boundaries. The combined effects enhance the thermal stability of the microstructure and micro-mechanical properties.

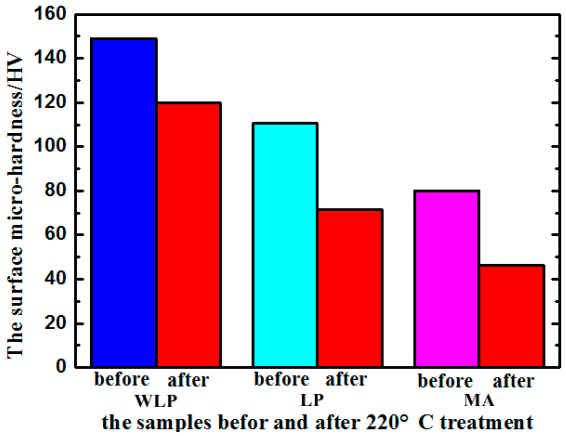

Figure 10. Surface micro-hardness of samples before and after aging.

3.4.3. Microstructure

From Figure 11, we can see that the grain size grew after aging compared with Figure 6. However, the growth rate of the grain size in the WLP-treated area is smaller. The average size of grain is about 55 μm for the WLP-treated area, while this value increases to about 95 μm (the yellow arrows point) and 200 μm for the LP-treated sample and the matrix, respectively.

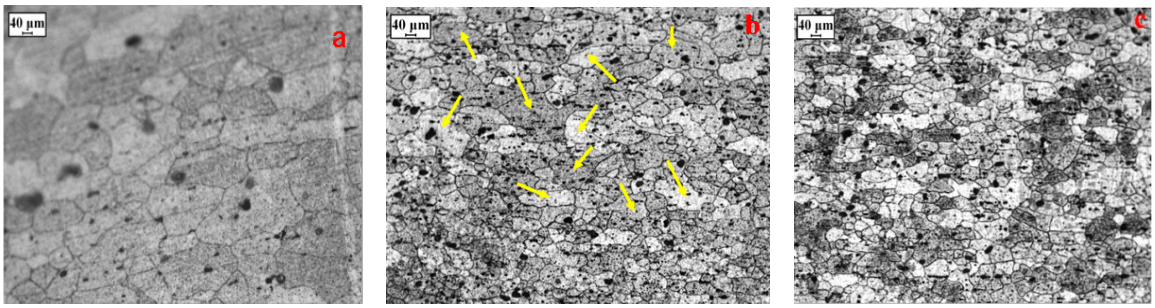

Figure 11. Microstructure of samples after aging: (**a**) matrix; (**b**) LP-treated (1.8 J + 25 °C); (**c**) WLP-treated (1.8 J + 120 °C).

The phenomenon can be explained by the stability of the dislocation. The dislocation induced by the WLP has an excellent thermal stability; after aging, the level of dislocation density is still high. In addition, the nano-precipitates are formed by DP during the WLP, and these nano-precipitates also have good thermal stability. The interaction between these nano-precipitates and the dislocation results in a further improvement of the thermal stability of the dislocation. According to Equation (2) [27]:

$$d = \frac{k}{\sqrt{\rho}} \tag{2}$$

where d is the grain size, ρ is the dislocation density, k is the materials coefficient; the higher the dislocation density, the smaller the grain size, so the grain size of the WLP-treated sample was still refined after aging.

4. Conclusions

(1) The surface residual compressive stress induced by WLP decreases with the increase of temperature. The micro-hardness increases initially, and then decreases with the increasing temperature. The depth of the hardening layer increases with the increasing temperature.

(2) The WLP process can further refine the grain size compared to the LP process due to the dynamic strain aging effect. The Si particles are significantly refined and balled in SEM morphologies for both LP- and WLP-treated samples.

(3) After aging for 100 min at 220 °C, the residual compressive stress and micro-hardness induced by WLP reveal an excellent thermal stability, only decreasing by 23.31% and 19.70%, respectively.

Acknowledgments: The authors are grateful for the support provided by University Graduate Scientific Research Innovation Project of Jiangsu Province (No. CXZZ12_0659).

Author Contributions: H. Chen and J. Zhou conceived and designed the experiments; H. Chen and X. Xie performed the experiments; H. Chen and S. Huang analyzed the data; J. Sheng and X. Meng contributed materials and analysis tools; H. Chen and J. Sheng wrote the paper.

Conflicts of Interest: The authors declare no conflict of interest.

References

1. Zhu, M.; Jian, Z. Effects of T6 heat treatment on the microstructure, tensile properties, and fracture behavior of the modified A356 alloys. *Mater. Des.* **2009**, *36*, 243–249. [CrossRef]
2. Ceschini, L.; Morri, A. Predictive equations of the tensile properties based on alloy hardness and microstructure for an A356 gravity die cast cylinder head. *Mater. Des.* **2011**, *32*, 1367–1375. [CrossRef]
3. Baradarani, B.; Raiszadeh, R. Precipitation hardening of cast Zr-containing A356 aluminum alloy. *Mater. Des.* **2011**, *32*, 935–940. [CrossRef]
4. Dobrzanski, L.A.; Borek, W.; Maniara, R. Influence of the crystallization condition on Al-Si-Cu casting alloys structure. *Mater. Manuf. Eng.* **2006**, *18*, 211–214.

5. Hirsch, J.; Al-Samman, T. Superior light metals by texture Engineering: Optimized aluminum and magnesium alloys for Automotive applications. *Acta Mater.* **2013**, *61*, 818–843. [CrossRef]
6. Molina, R.; Leghissa, M.; Mastrogiacomo, L. New developments in high performance cylinder heads: Application of LHIP and split cylinder head concept. *Metall. Sci. Technol.* **2004**, *22*, 1–8.
7. Feicus, F.J. Optimization of Al-Si cast alloys for cylinder head applications. *AFS Trans.* **1998**, *106*, 225–231.
8. Wang, F.; Zhang, J.S.; Xiong, B.Q. Effect of Fe and Mn additions on microstructure and mechanical properties of spray-deposited Al-20Si-3Cu-1Mg alloy. *Mater. Charact.* **2009**, *60*, 384–388. [CrossRef]
9. Wang, Q.G. Plastic deformation behavior of aluminum casting alloys A356/357. *Metall. Mater. Trans. A* **2004**, *35A*, 2707–2718. [CrossRef]
10. Haghshenas, M.; Zarei-Hanzaki, A.; Fatemi-Varzaneh, S.M. The effects of thermo-mechanical parameters on the microstructure of Thixocast A356 aluminum alloy. *Mater. Sci. Eng. A* **2008**, *480*, 68–74. [CrossRef]
11. Hwang, J.Y.; Doty, H.W.; Kaufman, M.J. The effects of Mn additions on the microstructure and mechanical properties of Al-Si-Cu casting alloys. *Mater. Sci. Eng. A* **2008**, *488*, 496–504. [CrossRef]
12. Miller, W.S.; Zhuang, L.; Bottema, J.; Wittebrood, A.J.; DeSmet, P.; Haszler, A.; Vieregge, A. Recent development in aluminum alloys for the automotive industry. *Mater. Sci. Eng. A* **2000**, *280*, 37–49. [CrossRef]
13. Cho, K.T.; Yoo, S.; Lim, K.M.; Kim, H.S.; Lee, W.B. Effect of Si content on surface hardening of Al-Si alloy by shot peening treatment. *J. Alloys Compd.* **2011**, *509*, S265–S270. [CrossRef]
14. Chang, H.-W.; Kelly, P.M.; Shi, Y.-N.; Zhang, M.-X. Effect of eutectic Si on surface nanocrystallization of Al-Si alloys by surface mechanical attrition treatment. *Mater. Sci. Eng. A* **2011**, *530*, 304–314. [CrossRef]
15. Chang, H.-W.; Kelly, P.M.; Shi, Y.-N.; Zhang, M.-X. Thermal stability of nanocrystallized surface produced by surface mechanical attrition treatment in aluminum alloys. *Surf. Coat. Technol.* **2012**, *206*, 3970–3980. [CrossRef]
16. Mazaheri, Y.; Karimzadeh, F.; Enayati, M.H. A novel technique for development of A356/Al_2O_3 surface nano-composite by friction stir processing. *J. Mater. Process. Technol.* **2011**, *211*, 1614–1619. [CrossRef]
17. Lee, J.-M.; Kang, S.-B.; Han, J. Dry sliding wear of MAO-coated A356/20 vol. % SiCp composites in the temperature range 25–180 °C. *Wear* **2008**, *264*, 75–85. [CrossRef]
18. Liao, Y.; Ye, C.; Kim, B.-J.; Suslov, S.; Stach, E.A.; Cheng, G.J. Nucleation of highly dense nano-scale precipitates based on warm laser shock Peening. *J. Appl. Phys.* **2010**, *108*, 063518. [CrossRef]
19. Ye, C.; Liao, Y.; Cheng, G.J. Warm Laser shock Peening Driven Nanostructures and Their Effects on Fatigue Performance in Al Alloy 6061. *Adv. Eng. Mater.* **2010**, *12*, 291–297.
20. Cottrell, A.H. LXXXVI. A note on the Portevin-Le Chatelier effect. *Philos. Mag.* **1953**, *44*, 829. [CrossRef]
21. Ye, C.; Suslov, S.; Kim, B.J.; Stach, E.A.; Cheng, G.J. Fatigue performance improvement in AISI 4140 steel by dynamic strain aging and dynamic precipitation during warm laser shock peening. *Acta Mater.* **2011**, *59*, 1014–1025. [CrossRef]
22. Ye, C.; Cheng, G.J. Effects of temperature on laser shock induced plastic deformation: The case of cooper. *J. Manuf. Sci. Eng.* **2010**, *132*, 061009. [CrossRef]
23. Liao, Y.; Suslov, S.; Ye, C.; Cheng, G.J. The mechanisms of thermal engineered laser shock peening for enhanced fatigue performance. *Acta Meter.* **2012**, *60*, 4997–5009. [CrossRef]
24. Xu, Z.; Fan, Z. A phenomenological Experimental of the Variation of Elastic Modulus with Temperature. *J. Southwest Jiaotong Univ.* **1993**, *3*, 88–92.
25. Matlock, D.K.; Richards, M.D.; Speer, J.G.; Alogab, K.A. Surface Modification to enhance Fatigue of Steel: Applications of Deep Rolling. *Mater. Sci. Forum* **2010**, *638–642*, 142–147. [CrossRef]
26. Li, H.Q.; Xing, D.M.; Tong, J.W.; Wang, S.B.; Yue, C. Relationship between yield stress and microcosmic structure of nanostructured material. *J. Tianjin Univ.* **2000**, *33*, 671–674.
27. Estrin, Y.; Tóth, L.S.; Molinari, A.; Bréchet, Y. A dislocation-based model for all hardening stages in large strain deformation. *Acta Mater.* **1998**, *46*, 5509–5522. [CrossRef]